

# Ground State of the Two Orbital Hubbard Model on the Pyrochlore Lattice with Competing Double Exchange and Superexchange Interactions

Nyayabanta Swain and Pinaki Majumdar

Harish-Chandra Research Institute, Chhatnag Road, Jhusi, Allahabad 211019, India

Homi Bhabha National Institute, Training School Complex, Anushakti Nagar, Mumbai 400085, India

(Dated: January 27, 2023)

The two orbital Hubbard model, with the electrons additionally coupled to a complex magnetic background, arises in the pyrochlore molybdates. The background involves local moments Hund's coupled to the electrons, driving double exchange ferromagnetism, and antiferromagnetic tendency arising from competing superexchange. The key scales include the Hubbard repulsion and the superexchange, both of which can be tuned in these materials, controlling phase transitions from a ferromagnetic metal to a spin glass metal and then a spin glass (Mott) insulator. We provide a comprehensive description of the ground state of this model using an unrestricted Hartree-Fock scheme implemented via a simulated annealing procedure. We establish the metal-insulator transition line for varying Hubbard interaction and superexchange. The orbital disorder already present in the ferromagnetic case is further enhanced by antiferromagnetic coupling and the resulting magnetic disorder. This suppresses the kinetic energy and shifts the metal-insulator transition to lower Hubbard interaction. We characterise the changing nature of the metal-insulator transition by tracking the magnetic and orbital correlations and the density of states. While this paper is focused on the ground state, a companion paper will discuss the finite temperature physics involving magnetic and orbital thermal fluctuations.

Keywords: Mott transition, pyrochlore, geometric frustration, double exchange

## I. INTRODUCTION

The most commonly studied Mott problem<sup>1</sup> involves the single band Hubbard model on a bipartite lattice<sup>2</sup>. In such a model, typically, nesting features drive a transition<sup>3</sup> to an antiferromagnetic insulating state at arbitrarily weak interaction - masking the 'Mott' effect. One can certainly study frustrated lattices<sup>4</sup>, which suppress magnetic order, and there is much work<sup>5-8</sup> on the triangular lattice Hubbard model. This is both an important model problem<sup>9</sup> and also a starting point for the layered organics<sup>10-13</sup>. Other frustrated lattices include the Kagome<sup>14</sup> in two dimensions (2D) and the FCC and pyrochlore lattices<sup>15</sup> in 3D. These are all harder problems than the square (or cubic) lattice since there is no longer any obvious magnetic order to simplify the correlated problem. These lattices, overall, provide interesting variation from the bipartite case because (i) the metal-insulator transition could occur in the background of short-range magnetic correlation, and (ii) the deep Mott insulating state itself could be a spin liquid<sup>16</sup>.

It would be vital to have experimental realisations to test out the predictions of the frustrated Mott studies. While there is significant effort in analysing the quasi 2D  $\kappa$ -BEDT organics<sup>10-13</sup> in terms of the triangular lattice, 3D realisations of 'Hubbard physics' on a frustrated structure are rare. Materials like the manganites<sup>17</sup> do involve strong correlation effects (and much else) but are on a bipartite structure - with relatively simple magnetic order. In this situation the discovery of the rare-earth (R) based pyrochlores, the molybdates<sup>18-22</sup>,  $R_2Mo_2O_7$ , and the iridates<sup>23-26</sup>,  $R_2Ir_2O_7$ , provided a breakthrough. Both these families show a metal-insulator transition as the rare-earth radius  $r_R$  is reduced<sup>21-24</sup>. There are, however, key differences (i) in terms of degrees of freedom and couplings, with respect to the Hubbard model, and (ii) the magnetic state that emerges in these two families.

Being 4d and 5d systems, respectively, both molybdates and iridates involve multiple bands. In the molybdate case this can be reduced to one itinerant electron in two degenerate orbitals. These electrons have an inter-orbital Hubbard repulsion and are also Hund's coupled to a  $S = 1/2$  local moment at each Mo site<sup>27</sup>. For the iridates one can motivate the use of an effective single band model which involve strong spin-orbit coupling in addition to the Hubbard interaction<sup>28</sup>. While both families show a 'Mott' transition, for the molybdates this happens in a somewhat spin disordered background, with no long range order in the insulating state<sup>15,18,19</sup>, while the iridates generally show a transition from a paramagnetic metal to an 'all-in-all-out' magnetic insulator<sup>29-31</sup>. The frustration in the pyrochlore lattice plays a role in both these materials, but one clearly requires more than the simple Hubbard model to approach the phenomena.

This paper is focused on a detailed study of the model appropriate to the molybdates  $R_2Mo_2O_7$ . These exhibit ground states that vary from a ferromagnetic metal (FM-M) to a spin glass metal (SG-M) and then a spin glass insulator (SG-I) as the rare earth radius is reduced<sup>32,33</sup>. Materials with  $R = Nd$  and  $Sm$  are metallic,  $R = Tb, Dy, Ho, Er,$  and  $Y$  are insulating, and  $R=Gd$  is on the verge of the insulator-metal transition<sup>33,34</sup> (IMT). The highest ferromagnetic  $T_c$  is  $\sim 100K$ , in  $Nd$ , while the spin glass transition temperature,  $T_{SG}$  is typically<sup>35-37</sup>  $\sim 20K$ . The unusual features in transport include very large residual resistivity,  $\sim 10 m\Omega cm$  close to the metal-insulator transition<sup>34</sup>, prominent anomalous Hall effect in metallic samples<sup>38-42</sup>, *e.g.*  $Nd_2Mo_2O_7$ , and magnetic field driven metallisation in the weakly insulating samples<sup>43</sup> *e.g.*  $Gd_2Mo_2O_7$ .

We will discuss the model for the molybdates in detail later, to motivate our study it suffices to mention that the active degrees of freedom include one electron per Mo in a twofold degenerate orbital, Hund's coupled to a  $S = 1/2$  moment on the same ion. The electrons have onsite Hubbard repulsion ( $U$ )

between them while the local moments have a nearest neighbour antiferromagnetic coupling,  $J_{AF}$ . The Hund's coupling drives double exchange (DE) ferromagnetism, opposed by AF superexchange, while Hubbard repulsion promotes a Mott insulating state. Reducing  $r_R$  reduces the hopping - weakening DE and also enhancing the effect of Hubbard repulsion, while increasing pressure is supposed to (mainly) affect<sup>22</sup> the antiferromagnetic coupling.

There are several major questions left unresolved by existing work: (1) At ambient pressure the metal-insulator and magnetic 'transition' are simultaneous, is that true with increasing pressure (changing  $J_{AF}$ ) as well? (2) Is there an 'universal' quantity that dictates the MIT trajectory over a large pressure window? (3) What is the fate of the coupled spin-orbital state for changing pressure and rare earth radius? (4) What is the low energy spectral behaviour in the vicinity of the MIT as the pressure is varied? (5) What is the quasiparticle character close to the Mott transition? (6) Can we obtain realistic thermal scales for the magnetic transitions?

We employ a real space approach, equivalent to unrestricted Hartree-Fock at zero temperature, that uses a static auxiliary orbital field to handle the Hubbard interaction. We solve the resulting 'electron - local moment - orbital moment' problem via Monte Carlo based simulated annealing on the pyrochlore lattice. Within the limits of our method we address (1)-(4) of the questions posed above, and (5) and (6) elsewhere. Our main results are the following:

(i) *Phase boundaries*: The proximity of the MIT and magnetic transitions in the ambient pressure molybdates is a coincidence, at weak AF coupling the metal and insulator are both ferromagnetic, while at strong AF coupling they are both spin disordered. (ii) *Physics behind the MIT*: The shift in the critical interaction for the MIT, with applied pressure, can be understood in terms of the kinetic energy suppression driven by growing spin and orbital disorder. (iii) *Coupled spin-orbital state*: The magnetic state is a spin ferromagnet (S-F) or a spin liquid (S-L), the orbital state is similarly O-F or O-L. We find that the low  $J_{AF}$  state is mainly S-F - O-F while the large  $J_{AF}$  state is S-L -O-L. The exception is the large  $U$  state at small  $J_{AF}$  which is S-F but O-L. (iv) *Spectral behaviour near the MIT*: The  $U_c$  changes with changing  $J_{AF}$ , so we use a normalised frequency scale,  $\omega/U_c(J_{AF})$ , to compare spectral features. At the MIT the larger  $J_{AF}$  systems have more low energy spectral weight than the weak  $J_{AF}$  case. Surprisingly, the gap edge states at large  $J_{AF}$  are strongly localised, leading to an optical gap that is larger than the density of states gap, revealing the growing Anderson character of the transition with increasing  $J_{AF}$ .

This paper is one of a two part study of the two orbital magnetic phase competing model appropriate to the molybdates. This paper, Paper I, focuses on the ground state, Paper II will discuss thermal phase transitions. Although focused on the ground state, most of the introductory and methodological issues are discussed in this paper, and not repeated in Paper II. In the next section we discuss the auxiliary field based Monte Carlo method, indicating its relation to full fledged quantum Monte Carlo and the unrestricted Hartree-Fock methods. This is followed by a discussion of the results, including the ground

state phase diagram, the detailed magnetic and orbital structure factors in the different phases, and the density of states and transport properties across the metal-insulator transition.

## II. MODEL AND METHOD

### A. Model

The  $R_2Mo_2O_7$  structure consists of two interpenetrating pyrochlore lattices, one formed by Mo cations and the other by R. Model Hamiltonian studies ignore the orbitals on R and oxygen, focusing instead on the orbitals on Mo. The Mo atom has octahedral oxygen coordination, the resulting crystal field splits the fivefold degenerate Mo 4d states into doubly degenerate  $e_g$  and triply degenerate  $t_{2g}$  manifolds, and a trigonal distortion splits the  $t_{2g}$  further into a nondegenerate  $a_{1g}$  and a doubly degenerate  $e'_g$ . The hopping matrix elements between Mo orbitals at different sites is dictated by the intervening oxygen. The Mo cation is nominally tetravalent and has two electrons on average. The deeper  $a_{1g}$  state behaves like a local moment, and the single electron in the two  $e'_g$  orbitals is the 'itinerant' degree of freedom<sup>27</sup>. The  $e_g$  state remains unoccupied.

There are additional small scales, related to bond distortions, *etc*, that are responsible for the spin freezing phenomena<sup>44,45</sup>. We ignore them for the time being. Also, the moments on R can be relevant when studying effects like spin chirality induced anomalous Hall effect<sup>38-42</sup>. We do not include these moments in our model.

We study the following model<sup>46</sup>, in parameter regimes described below:

$$H = \sum_{\langle ij \rangle, \alpha\beta, \sigma} t_{ij}^{\alpha\beta} c_{i\alpha\sigma}^\dagger c_{j\beta\sigma} - J_H \sum_{i, \alpha} \mathbf{S}_i \cdot c_{i\alpha\sigma}^\dagger \vec{\sigma}_{\sigma\sigma'} c_{i\alpha\sigma'} + J_{AF} \sum_{\langle ij \rangle} \mathbf{S}_i \cdot \mathbf{S}_j + \sum_{i, \alpha\beta\alpha'\beta'}^{\sigma, \sigma'} U_{\alpha\beta}^{\alpha'\beta'} c_{i\alpha\sigma}^\dagger c_{i\beta\sigma'}^\dagger c_{i\beta\sigma'} c_{i\alpha\sigma}$$

The first term is the kinetic energy, involving nearest neighbour intra and inter-orbital  $e'_g$  hopping. The second term is the Hund's coupling between the  $a_{1g}$  local moment  $\mathbf{S}_i$  and the  $e'_g$  electrons,  $J_{AF}$  is the AF superexchange coupling between local moments at neighbouring sites on the pyrochlore lattice, and the  $U$  represent onsite  $e'_g$  Coulomb matrix elements.

To simplify the computational problem we treat the localized spins  $\mathbf{S}_i$  as classical unit vectors, absorbing the size  $S$  in the magnetic couplings. We will comment on the limitations of this approximation later. Also, to reduce the size of the Hilbert space we assume that  $J_H/t \gg 1$ , where  $t$  is the typical hopping scale, so that only the locally 'spin aligned' fermion state is retained. In this local basis the hopping matrix elements are dictated by the orientation of the  $\mathbf{S}_i$  on neighbouring sites. This leads to the simpler model:

$$H = \sum_{\langle ij \rangle, \alpha\beta} \tilde{t}_{ij}^{\alpha\beta} \tilde{c}_{i\alpha}^\dagger \tilde{c}_{j\beta} + J_{AF} \sum_{\langle ij \rangle} \mathbf{S}_i \cdot \mathbf{S}_j + U \sum_i^{\alpha \neq \beta} n_{i\alpha} n_{i\beta}$$

where the fermions are now ‘spinless’.  $U > 0$  is the inter-orbital Hubbard repulsion. The effective hopping is determined by the orientation of the localized spins  $\mathbf{S}_i = (\sin\theta_i \cos\phi_i, \sin\theta_i \sin\phi_i, \cos\theta_i)$ , as  $t_{ij}^{\alpha\beta} = [\cos\frac{\theta_i}{2} \cos\frac{\theta_j}{2} + \sin\frac{\theta_i}{2} \sin\frac{\theta_j}{2} e^{-i(\phi_i - \phi_j)}] t^{\alpha\beta}$ , with  $t^{11} = t^{22} = t$  and  $t^{12} = t^{21} = t'$ . We set  $t' = 1.5t$  as is appropriate for these kinds of orbitals<sup>27</sup>.

The first two terms represent fermions in a classical spin background and the resulting magnetic phase competition has been studied on a pyrochlore<sup>47</sup>. While these results are interesting they miss out on the large correlation scale,  $U$ , that drives the Mott transition. One option is to treat the model within dynamical mean field theory (DMFT)<sup>48</sup>, but then the spatial character crucial to the pyrochlore lattice is lost.

The current paper is focused on the ground state but we discuss our general strategy for solving the finite temperature problem below. This will set the stage for the finite  $T$  results in Paper II, and also describe the simulated annealing scheme for arriving at the ground state.

## B. Method

We handle the problem in real space as follows: (i) We use a Hubbard-Stratonovich (HS)<sup>49–51</sup> transformation that decouples  $Un_{i\alpha}n_{i\beta}$  in terms of an auxiliary orbital variable  $\Gamma_i(\tau)$ , coupling to the electronic orbital moment  $\mathbf{O}_i = \sum_{\mu\nu} c_{i\mu}^\dagger \vec{\sigma}_{\mu\nu} c_{i\nu}$ , and a scalar field  $\Phi_i(\tau)$  coupling to the electronic density  $n_i$  at each site. The Matsubara frequency versions of these fields are  $\Gamma_{i,n}$  and  $\Phi_{i,n}$ , where  $\Omega_n = 2\pi nT$  is a bosonic frequency. (ii) An exact treatment of the resulting functional integral, see below, requires quantum Monte Carlo (QMC) - computing a fermion determinant  $D(\Gamma_{i,n}, \Phi_{i,n}, \mathbf{S}_i)$  iteratively as the ‘weight factor’ for auxiliary field configurations. Fermion Green’s functions would be computed on the equilibrium  $\{\Gamma, \Phi, \mathbf{S}\}$  backgrounds.

The QMC implementation, which we will approximate, takes the following route. The partition function is written as a functional integral over Grassmann fields  $\psi_{i\alpha}(\tau)$  and  $\bar{\psi}_{i\alpha}(\tau)$ :

$$Z = \int \mathcal{D}\psi \mathcal{D}\bar{\psi} \mathcal{D}\mathbf{S} e^{-\int_0^\beta d\tau \mathcal{L}(\tau)}$$

$$\mathcal{L}(\tau) = \sum_{\langle ij \rangle, \alpha\beta} \{ \bar{\psi}_{i\alpha} ((\partial_\tau - \mu)\delta_{ij}\delta_{\alpha\beta} + \tilde{t}_{ij}^{\alpha\beta}) \psi_{j\beta} \}$$

$$+ U \sum_{i, \alpha \neq \beta} \bar{\psi}_{i\alpha} \psi_{i\alpha} \bar{\psi}_{i\beta} \psi_{i\beta} + J_{AF} \sum_{\langle ij \rangle} \mathbf{S}_i \cdot \mathbf{S}_j$$

The quartic term is ‘decoupled’ exactly via a Hubbard-Stratonovich transformation

$$e^{U \bar{\psi}_{i\alpha} \psi_{i\alpha} \bar{\psi}_{i\beta} \psi_{i\beta}} = \int \frac{d\Phi_i d\Gamma_i}{4\pi^2 U} e^{(i\Phi_i n_i - \Gamma_i \cdot \mathbf{O}_i + \frac{\Phi_i^2}{U} + \frac{\Gamma_i^2}{U})}$$

where  $\Phi_i(\tau)$  and  $\Gamma_i(\tau)$  are two auxiliary fields:  $\Phi_i(\tau)$  coupling to charge density  $n_i = n_{i\alpha} + n_{i\beta}$ , and  $\Gamma_i(\tau)$  coupling to the orbital variable  $\mathbf{O}_i = \sum_{\mu\nu} \psi_{i\mu} \vec{\sigma}_{\mu\nu} \psi_{i\nu}$ . This leads to:

$$Z = \int \mathcal{D}\psi \mathcal{D}\bar{\psi} \mathcal{D}\mathbf{S} \prod_i \frac{d\Phi_i d\Gamma_i}{4\pi^2 U} e^{-\int_0^\beta d\tau \mathcal{L}(\tau)}$$

$$\mathcal{L}(\tau) = \mathcal{L}_0(\tau) + \mathcal{L}_{int}(\tau) + \mathcal{L}_{cl}(\tau)$$

$$\mathcal{L}_0(\tau) = \sum_{\langle ij \rangle, \alpha\beta} \{ \bar{\psi}_{i\alpha} ((\partial_\tau - \mu)\delta_{ij}\delta_{\alpha\beta} + \tilde{t}_{ij}^{\alpha\beta}) \psi_{j\beta} \}$$

$$\mathcal{L}_{int}(\tau) = \sum_i \{ i\Phi_i \bar{\psi}_{i\alpha} \psi_{i\beta} \delta_{\alpha\beta} - \Gamma_i \cdot \bar{\psi}_{i\alpha} \vec{\sigma}_i \psi_{i\beta} \}$$

$$\mathcal{L}_{cl}(\tau) = \sum_i \left\{ \frac{\Phi_i^2}{U} + \frac{\Gamma_i^2}{U} \right\} + J_{AF} \sum_{\langle ij \rangle} \mathbf{S}_i \cdot \mathbf{S}_j$$

Since the fermions are now quadratic the  $\int \mathcal{D}\Psi..$  integrals can be formally performed to generate the effective action for the background fields:

$$Z \sim \int \mathcal{D}\Phi \mathcal{D}\Gamma \mathcal{D}\mathbf{S} e^{-S_{eff}\{\Phi, \Gamma, \mathbf{S}\}}$$

$$S_{eff} = \log \text{Det}[\mathcal{G}^{-1}\{\Phi, \Gamma, \mathbf{S}\}] + \int_0^\beta d\tau \mathcal{L}_{cl}(\tau)$$

In the expression above  $\mathcal{G}$  is the electron Green’s function in a  $\{\Phi, \Gamma, \mathbf{S}\}$  background.

Now the options. (1) Quantum Monte Carlo would proceed by using  $S_{eff}$  as the ‘weight’ for the background configurations, and compute electron properties on these after equilibration. (2) Mean field theory would assume the fields to be time independent, replace them by their mean values, and minimise the free energy. (3) A *static path approximation* to  $Z$  again assumes the fields to be time independent, but samples over spatial fluctuations.

We adopt method (3), which is computationally simpler than QMC but much more sophisticated than MFT at finite temperature. So we (i) neglect the imaginary time dependence of  $\Phi_i$  and  $\Gamma_i$ , *i.e.*, retain only the zero Matsubara frequency modes of these fields, and (ii) replace  $\Phi_i$  by its saddle point value  $\langle \Phi_i \rangle = (U/2)\langle n_i \rangle = U/2$ , since the important low energy fluctuations arise from the  $\Gamma_i$ . The electron is now subject to *static* background fields so the partition function can be written as a trace over an effective ‘Hamiltonian’, rather than require an effective ‘action’. Specifically:

$$H_{eff}\{\Gamma_i, \mathbf{S}_i\} = -\frac{1}{\beta} \log \text{Tr} e^{-\beta H_{el}} + H_{AF} + \frac{1}{U} \sum_i \Gamma_i^2$$

$$H_{el} = \sum_{ij} \tilde{t}_{ij}^{\alpha\beta} c_{i\alpha}^\dagger c_{j\beta} - \tilde{\mu} \sum_i n_i - \sum_i \Gamma_i \cdot \mathbf{O}_i$$

with  $\tilde{\mu} = \mu - U/2$  and  $H_{AF}$  the Heisenberg term. For convenience we redefine  $\Gamma_i \rightarrow \frac{U}{2} \Gamma_i$ , so that the  $\Gamma_i$  is dimensionless. This leads to the effective electronic Hamiltonian used in the text:

$$H_{el} = \sum_{ij} \tilde{t}_{ij}^{\alpha\beta} c_{i\alpha}^\dagger c_{j\beta} - \tilde{\mu} \sum_i n_i - \frac{U}{2} \sum_i \Gamma_i \cdot \mathbf{O}_i$$

The localized spin and orbital moment configurations follow the distribution

$$P\{\mathbf{S}_i, \Gamma_i\} \propto \text{Tr}_{cc^\dagger} e^{-\beta H_{eff}}$$

This overall approach has been used in the nuclear many body problem<sup>52,53</sup>, superconductivity<sup>54,55</sup>, *etc.*, and by us in other studies of the Mott problem before<sup>56</sup>.

There are regimes where some analytic progress can be made, as we discuss later, but our results are based on a Monte Carlo solution of the model above - generating the equilibrium configuration for the  $\{\mathbf{S}_i, \mathbf{\Gamma}_i\}$  through iterative diagonalisation of  $H_{eff}$ . We start with high temperature,  $\sim 0.5t$ , higher than any transition temperature in the problem, and reduce it to  $T = 0.001t$  to access ground state properties. To access large sizes within reasonable time we use a cluster algorithm<sup>57</sup> for estimating the update cost. Results in this paper are for a  $6 \times 6 \times 6$  pyrochlore lattice of  $\sim 800$  atoms.

A couple of comments on the  $T \rightarrow 0$  limit of our method which reduces to unrestricted Hartree-Fock in the magnetic channel. Traditionally, Hartree-Fock calculations impose a certain pattern on the order parameter and minimise with respect to the amplitude. On a frustrated geometry it is not clear what pattern to impose so we vary with respect to the full set  $\{\mathbf{S}_i, \mathbf{\Gamma}_i\}$ . The resulting state turns out to be disordered but correlated, and leads to a non trivial electronic spectrum.

### C. Observables

From the equilibrium configurations obtained at the end of annealing we calculate the following averaged quantities (angular brackets represent thermal average over MC configurations): (i) Magnetic and orbital structure factors are:

$$S_{mag}(\mathbf{q}) = \frac{1}{N^2} \sum_{ij} \langle \mathbf{S}_i \cdot \mathbf{S}_j \rangle e^{i\mathbf{q} \cdot (\mathbf{r}_i - \mathbf{r}_j)}$$

$$S_{orb}(\mathbf{q}) = \frac{1}{N^2} \sum_{ij} \langle \mathbf{\Gamma}_i \cdot \mathbf{\Gamma}_j \rangle e^{i\mathbf{q} \cdot (\mathbf{r}_i - \mathbf{r}_j)}$$

(ii) The size distribution of the orbital field is computed as

$$P(\Gamma) = \frac{1}{N} \sum_i \langle \delta(\Gamma - |\mathbf{\Gamma}_i|) \rangle$$

(iii) The electronic density of states is,

$$N(\omega) = \frac{1}{N} \sum_n \langle \delta(\omega - \epsilon_n) \rangle$$

where  $\epsilon_n$  are single particle eigenvalues in an equilibrium configuration.

## III. RESULTS

### A. Phase diagram

Fig.1(a) shows the ground state of the model for varying  $U/t$  and  $J_{AF}/t$ , while Fig.1(b) shows  $N(0)$ , the density of states at the Fermi level, over the same parameter space.

First the notation: we characterise phases in terms of their spin and orbital character, S-L is spin liquid and S-F is a

spin ferromagnet. Similarly, O-L is orbital liquid, *etc.* These phases also need to be specified in terms of their transport character. To avoid a cluttered picture we have simply shown the insulator-metal boundary in the  $t/U - J_{AF}/t$  plane, the metal/insulator aspect can be inferred from it. The metal-insulator transition can be located from the vanishing of  $N(0)$ , and also from a calculation of the d.c conductivity (which we do not present in this paper).

When  $J_{AF} = 0$  there is a metal-insulator transition at  $U_c \sim 9t$  from a ferromagnetic metal to a *ferromagnetic insulator*. When the superexchange is moderate,  $J_{AF} \sim 0.2t$ , there is strong competition between ferromagnetism (S-F, mediated by double-exchange) and antiferromagnetic tendency. As a result there is a crossover from S-F to spin disordered (S-L) behaviour with increasing  $U/t$  roughly around the MIT, although weak ferromagnetism survives in the insulator. For strong superexchange,  $J_{AF} \gtrsim 0.5t$ , the antiferromagnetic tendency suppresses ferromagnetism completely and, as we will show, there is no magnetisation at any  $U/t$ . We have a spin liquid state at all  $U/t$ . In this large  $J_{AF}$  limit, a relatively weak Hubbard repulsion,  $U \sim 5t$ , is enough to drive the metal-insulator transition.

To get a feel for the changing magnetic state and the shifting MI transition point, it is useful to examine an approximate effective ‘spin only’ model. Consider the bond kinetic energy in a spin configuration  $\{\mathbf{S}_i\}$ . It is the product of an electronic average and a modulated hopping both of which depend on  $\{\mathbf{S}_i\}$ . The dependence of the spin overlap factor is explicit, it is simply:  $\sqrt{(1 + \mathbf{S}_i \cdot \mathbf{S}_j)/2}$ . The electronic average does not have an obvious expression in terms of the spins but, as a starting approximation, we can replace  $\langle c_{i\alpha}^\dagger c_{j\beta} \rangle$  by its thermal average<sup>58</sup>. The thermal average, please note, is not a spin configuration dependent quantity.

Under this assumption the kinetic energy term can be ap-

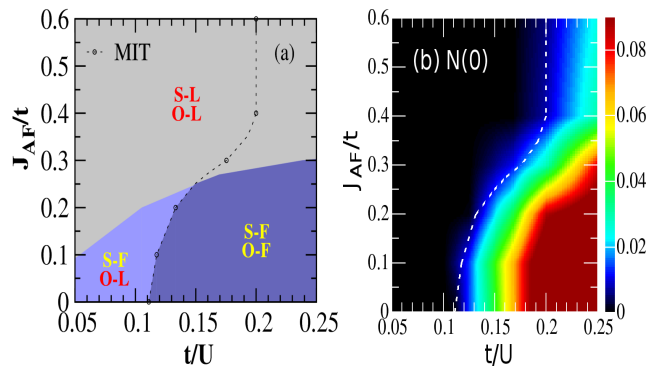


FIG. 1. (a) Ground state phase diagram showing the metal-insulator transition (MIT) boundary in the  $t/U$ , and  $J_{AF}/t$  plane. We label the various magnetic phases as spin-ferromagnet (S-F) and spin liquid (S-L). The two orbital phases are labeled as orbital-ferromagnet (O-F) and orbital liquid (O-L). The detailed characterisation of these phases is mentioned in the text. Panel (b) shows the density of states at the Fermi level,  $N(0)$ , for varying  $t/U$  and  $J_{AF}/t$ . The vanishing  $N(0)$  corresponds to the MIT (cross checked also with transport).

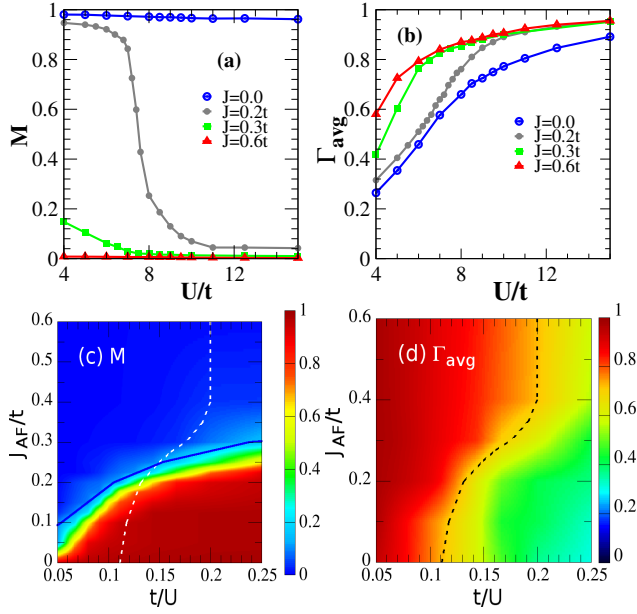


FIG. 2. Magnetisation ( $M$ ) and average orbital moment ( $\Gamma_{avg}$ ) in the ground state. (a)  $U/t$  dependence of  $M$  for several  $J_{AF}$ . At  $J_{AF} = 0$  the system has  $M = 1$  at all  $U$ , irrespective of metal/insulator character. For  $J_{AF} \gtrsim 0.5t$ ,  $M \sim 0$  for the entire  $U$  window probed. At intermediate  $J_{AF}$  the magnetisation has a rapid crossover around a scale  $U_{mag}(J_{AF})$  that is close to but not quite the metal-insulator transition point  $U_c(J_{AF})$ . (b) Shows the system averaged magnitude of the orbital moment  $\Gamma_{avg} = 1/N \sum_i |\Gamma_i|$ . For  $U/t \rightarrow \infty$ , the orbital moment  $\rightarrow 1$ , as one expects in the atomic limit. The approach to this asymptote is faster at larger  $J_{AF}$ . The  $U \rightarrow 0$  behaviour is dictated by the bandstructure, and change in the magnetic state with  $J_{AF}$ . (c)-(d) Overall variation of  $M$  and  $\Gamma_{avg}$  in the  $J_{AF}/t$  and  $t/U$  plane. The dashed line is the MIT boundary separating the metallic and insulating regimes.

proximated as below, and added to the AF term.

$$H_{eff}\{\mathbf{S}\} \approx \sum_{ij} D_{ij} \sqrt{(1 + \mathbf{S}_i \cdot \mathbf{S}_j)/2} + J_{AF} \sum_{\langle ij \rangle} \mathbf{S}_i \cdot \mathbf{S}_j$$

$$D_{ij} = \sum_{\alpha\beta} t_{ij}^{\alpha\beta} \langle c_{i\alpha}^\dagger c_{j\beta} + h.c \rangle$$

The role of the Hubbard interaction, acting through the orbital moment, is implicit in the model above. The  $D_{ij}$  are supposed to be computed in backgrounds that include the  $\Gamma_i$  as well as the AF coupling. Since the dependence of  $D_{ij}$  on the magnetic and orbital state is not known the model above does not have much predictive value. However, the thermally (and system) averaged  $D_{ij}$ , which we call just  $D$ , can serve to identify the origin of the changing magnetic character. It can also be related to direct measurables, *e.g.* (i) the spin stiffness (spin wave velocity), since the  $D$  and  $J_{AF}$  dictate this quantity, and (ii) the integrated optical weight, via the  $f$ -sum rule

$$\sum_{ij} D_{ij} \sqrt{(1 + \mathbf{S}_i \cdot \mathbf{S}_j)/2} \propto \int_0^\infty \sigma(\omega) d\omega \equiv n_{eff}$$

where  $n_{eff}$ , the integrated optical weight, is related to the effective carrier density. This can be roughly simplified to

$D\sqrt{1+m^2} \propto n_{eff}$ , where we have approximated the spin average by  $m^2$ . The physics content of this is simple - reducing magnetisation reduces the hopping ( $D$ ) and the combination determines  $n_{eff}$ .

### 1. The metal-insulator transition line

The role of  $J_{AF}$  is to generate magnetic phase competition and reduce the ferromagnetic tendency by suppressing the kinetic energy. To set a convenient reference, the effective bond resolved kinetic energy,  $D$ , at  $J_{AF} = 0$  and  $U \rightarrow 0$  is  $\sim -t$ . That allows us to set up three regimes.

(a). When  $J_{AF} \ll D$ , we essentially have a weakly renormalised FM ground state and  $U_c$  is only modestly suppressed with respect to the  $J_{AF} = 0$  value. For us this happens when  $J_{AF} \lesssim 0.1t$ . (b). In the interval  $0.1t < J_{AF} < 0.4t$  the  $U_c$  changes quickly, at  $J_{AF} = 0.4t$  it is roughly half the value at  $J_{AF} = 0$ . (c). For  $J_{AF} \gtrsim 0.4t$  the  $U_c$  does not reduce any further since the magnetic ground state is completely disordered and the magnetisation cannot be suppressed any further. This shows up as the vertical asymptote of the MIT line in Fig.1.

### 2. The ferromagnet to 'spin liquid' transition

The ferromagnet to spin liquid 'transition' occurs along a line that we call  $U_{mag}(J_{AF})$ . There is some ambiguity in locating this line since within our parameter space the magnetisation is always finite, if small. We set  $M = 0.05$  as the S-F to S-L transition. Just as  $U_c$  is dictated roughly by the competition between  $U$  and  $D$ ,  $U_{mag}$  is decided by the competition between  $J_{AF}$  and  $D$ .

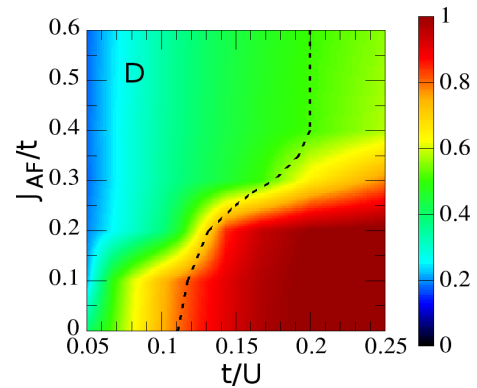


FIG. 3. The effective ferromagnetic exchange,  $D$ , at  $T = 0$  for varying  $t/U$  and  $J_{AF}/t$ . The calculation and significance of this quantity is explained in the text. The MIT boundary is shown by dotted lines and coincides with change from large to small values of  $D$ .

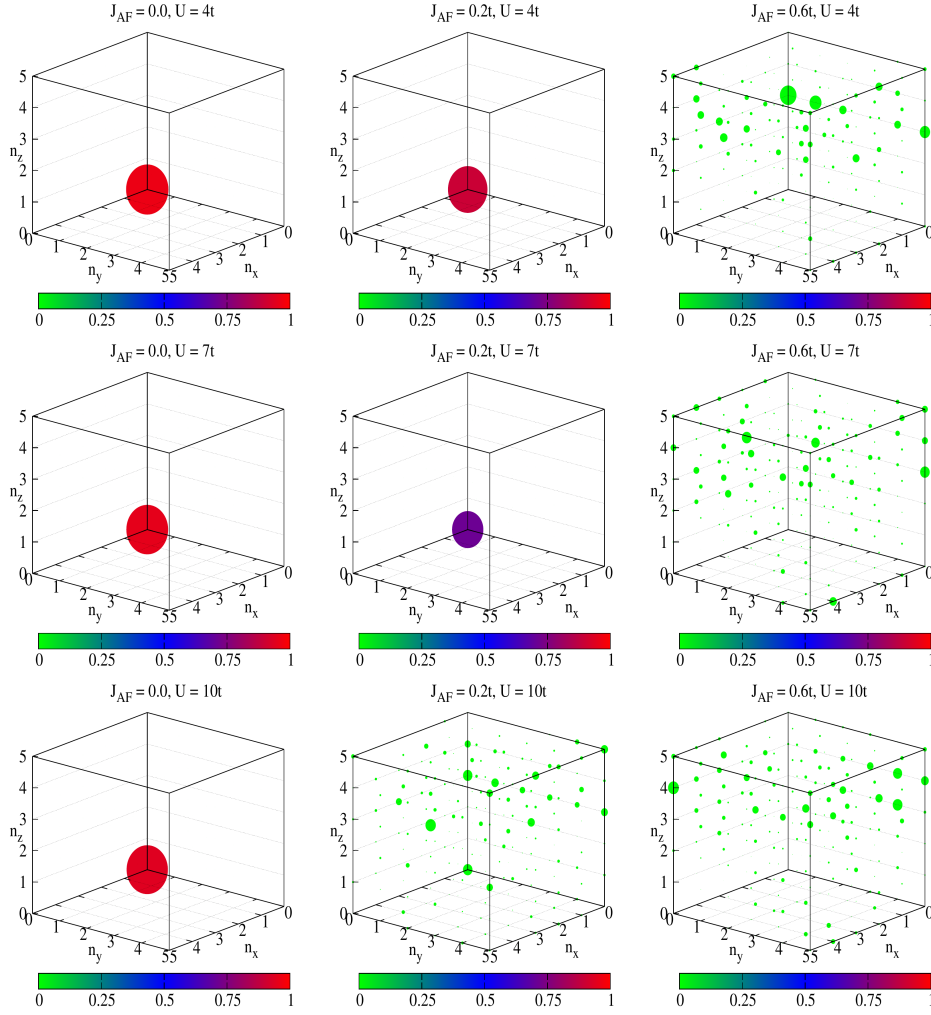


FIG. 4. Spin structure factor  $S_{mag}(\mathbf{q})$  at  $T = 0$  for  $U/t=4, 7$  and  $10$  for each of  $J_{AF} = 0$  (left column),  $0.2t$  (middle column) and  $0.6t$  (right column). We use the notation  $\mathbf{q} = \frac{2\pi}{L}(n_x, n_y, n_z)$ . The size of a dot signifies relative weight at a given  $\mathbf{q}$  while its color represents the actual magnitude of  $S_{mag}(\mathbf{q})$ . The presence of dominant weight at some  $\mathbf{q}$ , in these cases  $\mathbf{q} = (0, 0, 0)$  indicates magnetic order phase, while the ‘random’ but correlated patterns indicate a spin liquid.

### 3. Orbital character

The various orbital(O) phases obtained in our study are based on the orbital structure factor  $S_{orb}(\mathbf{q})$  calculation. For the orbital-ferromagnet phase  $S_{orb}(\mathbf{q})$  shows a peak at  $\mathbf{q} = (0, 0, 0)$  while for the orbital liquid phase it doesn’t show any peak at any  $\mathbf{q}$ .

### B. The magnetic state

A detailed understanding of the magnetic state is provided by the magnetic structure factor  $S_{mag}(\mathbf{q})$  computed in the optimised background. It highlights not only long range order, in terms of prominent peaks in  $\mathbf{q}$  space, but also possible correlations in the disordered state when there is no long range order.

Fig.4 shows  $S_{mag}(\mathbf{q})$  for three different superexchange

couplings and for three  $U$ ’s in each case. The  $U$ ’s are chosen so that they capture the metal, insulator, and crossover regime for all three values of  $J_{AF}$ .

For  $J_{AF} = 0$  there is no magnetic phase competition. At  $U = 4t$ ,  $S_{mag}(\mathbf{q})$  has dominant weight at  $\mathbf{q} = (0, 0, 0)$  describing the ferromagnetic order promoted by double-exchange. The magnetisation is  $\gtrsim 0.95$  (limited by our annealing process) and the structure factor peak is  $\sim 0.9 \sim M^2$ . As the row shows, this result does not depend on  $U$ , suggesting that even deep in the Mott insulator one would obtain a saturated ferromagnetic state. The  $T_c$ ’s would of course differ, as a separate paper would show, since the stiffness of the FM state depends on the kinetic energy - which is  $U$  dependent.

For  $J_{AF} = 0.2t$ ,  $S_{mag}(\mathbf{q})$  has a large weight at  $\mathbf{q} = (0, 0, 0)$  at  $U = 4t$ , as in the first row, but at  $U = 7t$  the peak, although still at  $(0, 0, 0)$ , has diminished weight,  $\sim 0.6$ . The metal-insulator transition occurs around  $U \sim 8t$  and by



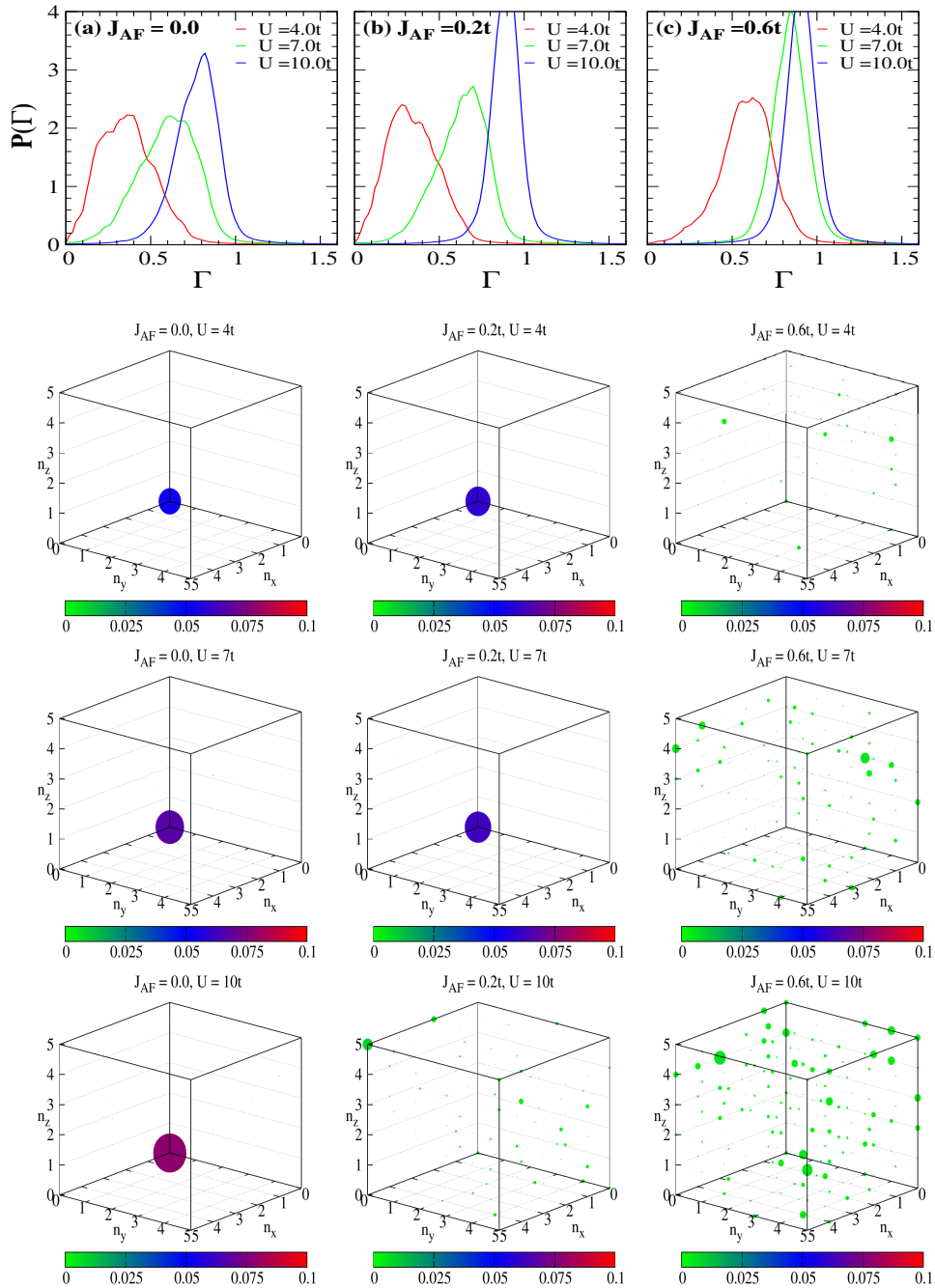


FIG. 5. (Top row) Ground state size distribution of the orbital field  $P(\Gamma)$  for  $J_{AF} = 0, 0.2t$  and  $0.6t$  for indicated  $U$  values. (Remaining rows) Orbital structure factor at  $T = 0$  for  $U/t = 4, 7$  and  $10$  for each of  $J_{AF} = 0$  (left column),  $0.2t$  (middle column) and  $0.6t$  (right column). We use the notation  $\mathbf{q} = \frac{2\pi}{L}(n_x, n_y, n_z)$ . The size of a dot signifies relative weight at a given  $\mathbf{q}$  while its color represents the actual magnitude of  $S_{mag}(\mathbf{q})$ . The presence of dominant weight at some  $\mathbf{q}$ , indicates a magnetic ordered phase, otherwise a disordered phase.

the time  $U = 10t$  (last row)  $S_{mag}$  does not have any prominent peaks at any  $\mathbf{q}$ . The superexchange coupling overcomes the kinetic energy gain from DE but the pyrochlore structure prevents AF ordering.

For  $J_{AF} = 0.6t$ ,  $S_{mag}(\mathbf{q})$  the weight is spread over all  $\mathbf{q}$  but in a correlated manner, indicative of a spin liquid phase.

### C. The orbital state

To have an idea of the underlying orbital state, we calculate the orbital structure factor  $S_{orb}(\mathbf{q})$ . Fig.5 shows the structure factor for the three superexchange couplings. For  $J_{AF} = 0$  we see  $S_{orb}(\mathbf{q})$  has dominant weight at  $\mathbf{q} = (0, 0, 0)$  describing the ferro-orbital (O-F) ordering. For  $J_{AF} = 0.2t$ ,  $S_{orb}(\mathbf{q})$

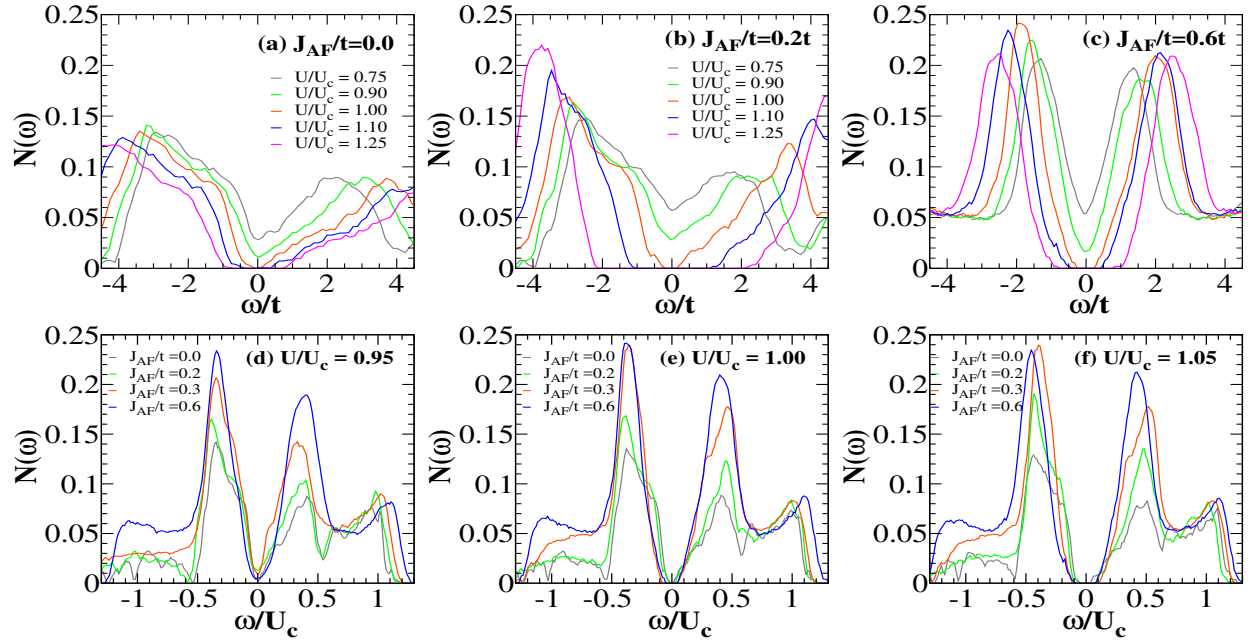


FIG. 6. (a)-(c) Ground state density of states (DOS) for  $J_{AF} = 0, 0.2t$  and  $0.6t$  for different  $U/U_c$ . (d) Ground state DOS at the Fermi level in the  $t/U$  and  $J_{AF}/t$  plane. (d)-(f) Ground state density of states (DOS) for  $U/U_c = 0.95, 1.0$  and  $1.05$ , on a normalised frequency scale, for the indicated  $J_{AF}$  values.

has dominant weight at  $\mathbf{q} = (0, 0, 0)$  for  $U = 4t$  and  $7t$  (O-F ordering), and an orbital liquid state for  $U = 10t$ . For  $J_{AF} = 0.6t$ ,  $S_{orb}(\mathbf{q})$  has weight spread over all  $\mathbf{q}$  indicating an orbital liquid state.

#### D. Density of states

Fig.6 shows the ground state DOS for various interaction strengths for the three regimes of superexchange interaction of our phase-diagram. We can see that for  $U < U_c$ , the DOS has a finite weight at the Fermi energy, and for  $U \geq U_c$ , the DOS has a gap in the spectrum. As  $U \rightarrow U_c$ , the DOS develops a prominent dip at the Fermi energy, a signature of the pseudogap (PG) phase. We can understand this in following way- the band ( $U = 0$ ) limit of this model is a metal, with finite DOS and a peak at the Fermi level. Inclusion of the inter-orbital interaction ( $U$ ) is treated as the emergence of orbital moments  $\Gamma_i$ , with the size of the orbital moment  $|\Gamma_i|$  is determined by the strength of  $U$ . For  $U < U_c$ , we have  $|\Gamma_i| \ll \Gamma_{sat} = 1$ . The presence of these orbital moments reduce the DOS at the Fermi level. As  $U \rightarrow U_c$ ,  $|\Gamma_i|$  increases monotonically and for  $U \gg U_c$  it saturates to the atomic value  $|\Gamma_i| = 1$ . The presence of large orbital moments for  $U \geq U_c$  leads to the opening of a gap in the DOS. From our calculation, we estimate that for  $J_{AF} = 0$ ,  $U_c = 9.0t$ , for  $J_{AF} = 0.2t$ ,  $U_c = 7.6t$  and for  $J_{AF} = 0.6t$ ,  $U_c = 5.0t$ . This indicates that the superexchange interaction favors the Mott-insulating phase.

The lower set of panels in Fig.6 show the DOS near the MIT for fixed ratios of  $U/U_c (J_{AF})$ . Within each panel the  $J_{AF}$  is varied to probe if the spectral behaviour changes with chang-

ing AF coupling, after factoring out the effect of  $U_c$  change by normalising the frequency axis by  $U_c$ . Our primary observation is that increasing  $J_{AF}$  leads to enhanced low energy DOS for a fixed ratio  $U/U_c$ . We attribute this to the increased spin and orbital disorder in the larger  $J_{AF}$  situation - leading to an increasing ‘Anderson-Mott’ character of the metal-insulator transition.

#### IV. CONCLUSION

In this paper we have studied the two orbital Hubbard model with the electrons additionally strongly coupled to a background local moment - and the moments interacting antiferromagnetically amongst themselves. This Hubbard-double exchange-superexchange scenario, on the pyrochlore lattice, is the minimal model for the rare earth molybdates. We map out the ground state phase diagram via a simulated annealing based unrestricted Hartree-Fock calculation and establish the metal-insulator and ferromagnet-spin liquid transition boundaries. We provide the detailed structure factors, and the density of states across the metal-insulator transition, pointing out an increasing Anderson-Mott character to the transition as the antiferromagnetic superexchange is increased. This effect should be readily observable in the high pressure experiments.

#### V. ACKNOWLEDGMENT

We acknowledge use of the HPC clusters at HRI.



- 
- <sup>1</sup> N. F. Mott, Proc. Roy. Soc. A **62**, 416 (1949); *Metal-Insulator Transitions*, Taylor and Francis (London) (1990).
- <sup>2</sup> M. Imada, A. Fujimori, and Y. Tokura, Rev. Mod. Phys. **70**, 1039 (1998).
- <sup>3</sup> J. E. Hirsch, Phys. Rev. B **31**, 4403 (1985).
- <sup>4</sup> L. Balents, Nature (London) **464**, 199 (2010).
- <sup>5</sup> Y. Imai and N. Kawakami, Phys. Rev. B **65**, 233103 (2002).
- <sup>6</sup> O. Parcollet, G. Biroli, and G. Kotliar, Phys. Rev. Lett. **92**, 226402 (2004).
- <sup>7</sup> B. Kyung and A.-M. S. Tremblay, Phys. Rev. Lett. **97**, 046402 (2006).
- <sup>8</sup> T. Ohashi, T. Momoi, H. Tsunetsugu, and N. Kawakami, Phys. Rev. Lett. **100**, 076402 (2008).
- <sup>9</sup> P. W. Anderson, Mater. Res. Bull. **8**, 153 (1973).
- <sup>10</sup> Y. Shimizu, et al. Phys. Rev. Lett. **91**, 107001 (2003).
- <sup>11</sup> M. Yamashita, et al. Nature Phys. **5**, 44 (2009).
- <sup>12</sup> K. Kanoda and R. Kato, Annu. Rev. Condens. Matter Phys. **2**, 167 (2011).
- <sup>13</sup> B. J. Powell and R. H. McKenzie, Rep. Prog. Phys. **74**, 056501 (2011).
- <sup>14</sup> Y. Imai, N. Kawakami, and H. Tsunetsugu, Phys. Rev. B **68**, 195103 (2003). N. Bulut, W. Koshibae, and S. Maekawa, Phys. Rev. Lett. **95**, 037001 (2005).
- <sup>15</sup> J. S. Gardner, M. J. P. Gingras, and J. E. Greedan, Rev. Mod. Phys. **82**, 53 (2010).
- <sup>16</sup> P. A. Lee, Journal of Physics: Conference Series **529**, 012001 (2014).
- <sup>17</sup> M. B. Salamon and M. Jaime, Rev. Mod. Phys. **73**, 583 (2001).
- <sup>18</sup> B. D. Gaulin, J. N. Reimers, T. E. Mason, J. E. Greedan, and Z. Tun, Phys. Rev. Lett. **69**, 3244 (1992).
- <sup>19</sup> M. J. P. Gingras, C. V. Stager, N. P. Raju, B. D. Gaulin, and J. E. Greedan, Phys. Rev. Lett. **78**, 947 (1997).
- <sup>20</sup> Y. Taguchi and Y. Tokura, Phys. Rev. B **60**, 10280 (1999).
- <sup>21</sup> I. Kezsmarki, et al., Phys. Rev. B **73**, 125122 (2006).
- <sup>22</sup> S. Iguchi, et al., Phys. Rev. Lett. **102**, 136407 (2009).
- <sup>23</sup> D. Yanagishima and Y. Maeno, J. Phys. Soc. Jpn. **70**, 2880 (2001).
- <sup>24</sup> K. Matsuhira, M. Wakeshima, Y. Hinatsu, and S. Takagi, J. Phys. Soc. Jpn. **80**, 094701 (2011).
- <sup>25</sup> M. Sakata, et al., Phys. Rev. B **83**, 041102 (2011).
- <sup>26</sup> F. F. Tafti, J. J. Ishikawa, A. McCollam, S. Nakatsuji, and S. R. Julian, Phys. Rev. B **85**, 205104 (2012).
- <sup>27</sup> I. V. Solovyev, Phys. Rev. B **67**, 174406 (2003).
- <sup>28</sup> B. J. Kim, et al., Phys. Rev. Lett. **101**, 076402 (2008).
- <sup>29</sup> K. Tomiyasu, et al., J. Phys. Soc. Jpn. **81**, 034709 (2012).
- <sup>30</sup> H. Sagayama, et al., Phys. Rev. B **87**, 100403(R) (2013).
- <sup>31</sup> S. M. Disseler, Phys. Rev. B **89**, 140413(R) (2014).
- <sup>32</sup> J. E. Greedan, et al., J. Solid State Chem. **68**, 300 (1987).
- <sup>33</sup> K. Miyoshi, et al., J. Magn. Magn. Mater. **226**, 898 (2001).
- <sup>34</sup> I. Kezsmarki, et al., Phys. Rev. Lett. **93**, 266401 (2004).
- <sup>35</sup> N. Ali, et al., J. Solid State Chem. **83**, 178 (1989).
- <sup>36</sup> N. Ali, et al., J. Alloys Compd. **181**, 281 (1992).
- <sup>37</sup> Y. Taguchi and Y. Tokura, Phys. Rev. B **60**, 10280 (1999).
- <sup>38</sup> T. Katsufuji, H.Y. Hwang and S.W. Cheong, Phys. Rev. Lett. **84**, 1998 (2000).
- <sup>39</sup> Y. Taguchi, et al., Science **291**, 2573 (2001).
- <sup>40</sup> Y. Taguchi, et al., Phys. Rev. Lett. **90**, 257202 (2003).
- <sup>41</sup> S. Iguchi, N. Hanasaki, and Y. Tokura, Phys. Rev. Lett. **99**, 077202 (2007).
- <sup>42</sup> K. Ueda, et al., Phys. Rev. Lett. **108**, 156601 (2012).
- <sup>43</sup> N. Hanasaki, et al., Phys. Rev. Lett. **96**, 116403 (2006).
- <sup>44</sup> T. E. Saunders and J. T. Chalker, Phys. Rev. Lett. **98**, 157201 (2007).
- <sup>45</sup> H. Shinaoka, Y. Tomita, and Y. Motome, Phys. Rev. Lett. **107**, 047204 (2011), Phys. Rev. B **90**, 165119 (2014).
- <sup>46</sup> Y. Motome and N. Furukawa, J. Phys.: Conf. Ser. **320**, 12060 (2011).
- <sup>47</sup> Y. Motome and N. Furukawa, Phys. Rev. Lett. **104**, 106407 (2010), Phys. Rev. B **82**, 060407(R) (2010).
- <sup>48</sup> A. Georges, et al., Rev. Mod. Phys. **68**, 13 (1996).
- <sup>49</sup> R. L. Stratonovich, Dokl. Akad. Nauk. SSSR **115**, 1097 (1957) (translation- Sov. Phys. Dokl. **2**, 416 (1958)); J. Hubbard, Phys. Rev. Lett. **3**, 77 (1959).
- <sup>50</sup> J. Hubbard, Phys. Rev. B **19**, 2626 (1979).
- <sup>51</sup> H. J. Schulz, Phys. Rev. Lett. **65**, 2462 (1990).
- <sup>52</sup> P. Arve, G. Bertsch, B. Lauritzen, and G. Puddu, Ann. Phys. **183**, 309 (1988).
- <sup>53</sup> B. Lauritzen, P. Arve, and G. F. Bertsch, Phys. Rev. B **61**, 2835 (1988).
- <sup>54</sup> M. Mayr, G. Alvarez, C. Sen, and E. Dagotto, Phys. Rev. Lett. **94**, 217001 (2005).
- <sup>55</sup> Y. Dubi, Y. Meir, and Y. Avishai, Nature, **449**, 876 (2007).
- <sup>56</sup> R. Tiwari and P. Majumdar, Europhys. Lett. **108**, 27007 (2014).
- <sup>57</sup> S. Kumar and P. Majumdar, Eur. Phys. J. B, **50**, 571 (2006).
- <sup>58</sup> S. Kumar and P. Majumdar, Eur. Phys. J. B, **46**, 315 (2005).